

# External and internal interface-controlled trimetallic PtCuNi nanoframes with high defect-density for enhanced electrooxidation of liquid fuels

*Daowei Gao<sup>a,b #</sup>, Shaohan Yang<sup>a #</sup>, Lifei Xi<sup>b</sup>, Marcel Risch<sup>b</sup>, Lianghao Song<sup>a</sup>, Yipin Lv<sup>a</sup>, Cuncheng Li<sup>a</sup>, Chunsheng Li<sup>a\*</sup>, Guozhu Chen<sup>a\*</sup>*

<sup>a</sup>School of Chemistry and Chemical Engineering, University of Jinan, Jinan 250022, PR. China.

<sup>b</sup>Helmholtz-Zentrum Berlin für Materialien und Energie GmbH, Nachwuchsgruppe Gestaltung des Sauerstoffentwicklungsmechanismus, Berlin 14109, Germany.

\*To whom correspondence should be addressed:

E-mail: [chm\\_lics@ujn.edu.cn](mailto:chm_lics@ujn.edu.cn); [chm\\_chengz@ujn.edu.cn](mailto:chm_chengz@ujn.edu.cn)

<sup>#</sup>Daowei Gao and Shaohan Yang contributed equally to this work.

## **Abstract**

Selectively exposing active surfaces of Pt-based nanoframes (NFs) can promote electrocatalysis of small organic molecules, especially regarding improved diffusion and anti-poisoning properties. However, the systematic investigation on the synthesis, as well as structure-property relationship, of Pt-based NFs with tunable external and internal surface structures is still at its early stage. Herein, we report a facile, environmental and one-pot approach to fabricate PtCuNi NFs with tunable external and internal surface structures by flexibly adjusting coordination and reducing agents. Interestingly, electrocatalytic results reveal that the PtCuNi NFs with variable external structures possess higher performance (activity and anti-CO-poisoning capability) than those with tunable internal structures as well as commercial Pt/C. Especially, the PtCuNi eb-NFs (external branch NFs) exhibit the excellent specific activities of methanol and formic acid electrooxidation reactions (MOR and FAOR), 10.7 and 7.9 times higher than those of commercial Pt/C, respectively. The PtCuNi eb-NFs also possess a superior diffusion ability for methanol electrooxidation (0.0276) and formic acid electrooxidation (0.0153) compared to other PtCuNi NFs with plentiful internal surface. The enhanced MOR and FAOR activities of PtCuNi eb-NFs are ascribed to its abundant external surface area and high defect-density (e.g. vacancy, subtle lattice distortion and high-index facets), which results in an optimal anti-CO-poisoning capability due to the diffusion and ligand effects. This work opens up a new pathway for enhancing the electrooxidation properties (anti-poisoning property and diffusion rate) of liquid fuels by tuning the surface structures of nanoframe catalysts.

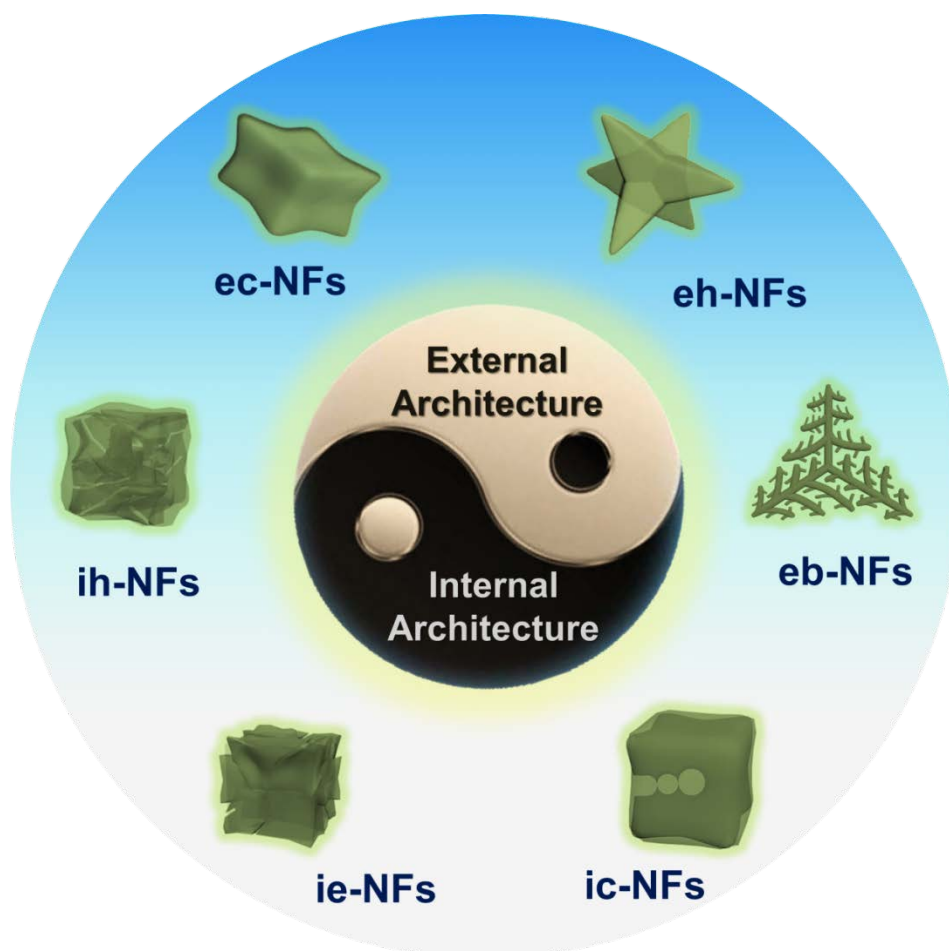
## 1 Introduction

Direct formic acid fuel cell (DFAFC) and direct methanol fuel cell (DMFC) with polymer electrolyte as membranes are the excellent energy conversion approaches because of their high energy yield as well as low pollution<sup>1-4</sup>. In spite of the speedy development of catalysts, the platinum (Pt) catalyst is still the most efficient catalyst in methanol and formic acid electrooxidation. However, Pt metal is quite expensive and easily poisoned by intermediate species (such as CO molecules) produced in formic acid and methanol electrooxidation process, which prevents its commercial application<sup>5-8</sup>. Therefore, how to design methanol and formic acid electrooxidation (MOR and FAOR) catalysts with high activity, low-cost and excellent poisoning resistance will be of great significance for DFAFC and DMFC.

Alloying with cheaper and more abundant transition metals are supposed as a universal strategy for enhancing the electrooxidation performance of Pt-based catalyst via the so-called ligand effect, that is, tuning the surface adsorption strength by electronic interaction between different metals<sup>9-13</sup>. To further enhance the utilization efficiency of Pt, several methods were developed in recent studies, such as selective exposure of desired facets and architectural engineering with promising nanostructures (e.g. polyhedrons<sup>14</sup>, hierarchical/ultrathin nanowires<sup>15, 16</sup>, nanosheets<sup>17, 18</sup>, nanodendrites<sup>19, 20</sup>, nanoframes (NFs)<sup>21, 22</sup>). Among them, NFs with open structure are demonstrated to be an ideal architecture to boost MOR and FAOR properties, because of their efficient Pt utilization and optimized mass transport within this unique structure<sup>23-25</sup>. Nevertheless, most of the previous works focus on the fabrication of NFs with novel structures, there is almost no research related to the design of NFs with tunable external and internal interface and the investigation of their effects on the properties of MOR and FAOR. The optimized external and internal interface of NFs can endow

excellent diffusion rate of poisonous species to the solution phase, which can restrain the adsorption of poisonous molecules (such as CO) on catalyst surface along with their high anti-poisoning property<sup>26-29</sup>. Moreover, the traditional synthesis of NFs usually involves the use of oleylamine (OAm) as the solvent and/or a time-consuming multi-step method, which is undesirable for industrial applications<sup>21, 30, 31</sup>. Therefore, the design of one-pot method to fabricate Pt-based (alloy) NFs with tunable external and internal surface structures and clarify their effects on MOR and FAOR properties is quite desirable, yet still a great challenge.

In this research, a one-pot method is reported to fabricate the trimetallic PtCuNi NFs with tunable surface structures both in external and internal interface in aqueous solution. The synthetic strategy (Scheme 1) is based on the wet-chemical reduction route including polyvinyl pyrrolidone (PVP), glycine, alcohol species, NaI, CuCl<sub>2</sub>, NiCl<sub>2</sub>, and H<sub>2</sub>PtCl<sub>6</sub>. The external and internal surface structures of PtCuNi NFs can be tuned via crystal growth control by using different amount of coordination agent and reductant. To the best of our knowledge, it is rarely reported that the external and internal interface structure of trimetallic NFs can be continuously tuned in an aqueous synthesis system. Specifically, the PtCuNi external branch NFs (PtCuNi eb-NFs) with optimized large specific surface area, 3-dimension structure, and abundant active defect sites have exhibited superior catalytic performances for methanol and formic acid electrooxidation in comparison with Pt/C catalyst. The structure-performance relationship between the PtCuNi NFs and the corresponding electrocatalytic properties (e.g. activity, anti-poisoning property and diffusion rate) has also been in-depth investigated.



**Scheme 1.** Schematic illustration of PtCuNi NFs with tunable external and internal architecture.

## 2 Experimental

### 2.1 Synthesis of PtCuNi NFs

Synthesis of PtCuNi NFs with tunable external structures. PtCuNi concave NFs (PtCuNi ec-NFs): Typically, 1.0 mL of  $\text{CuCl}_2$  solution (20.0 mM), 1.0 mL of  $\text{NiCl}_2$  solution (20.0 mM), 2.0 mL of  $\text{H}_2\text{PtCl}_6$  solution (19.3 mM), 0.7 mL of ethylene glycol, 150.0 mg of NaI, 200.0 mg of PVP, 303.4 mg of glycine were dissolved in a beaker and sonicated for 10.0 min, and further stirred for 12 h. The obtained solution was moved to a Teflon-lined autoclave. Then the mixture was heated to 200.0 °C and kept for 4 h. The final PtCuNi ec-NFs were obtained by centrifugation at 10000 rpm for 15.0 min, and continuous washed with a mixture of

deionized water, ethanol and acetone. The synthetic recipe of PtCuNi branch NFs (PtCuNi eb-NFs) is almost the same with that of PtCuNi ec-NFs except the glycine amount changing to 100.0 mg. The synthetic recipe of PtCuNi hexapod NFs (PtCuNi eh-NFs) is modified from that of ec-NFs, including the increase of NaI amount to 602.6 mg, and using ethanolamine (0.7 mL) instead of ethylene glycol.

Synthesis of PtCuNi NFs with tunable internal structures. PtCuNi cavity NFs (PtCuNi ic-NFs): Briefly, 1.0 mL of CuCl<sub>2</sub> solution (20.0 mM), 1.0 mL of NiCl<sub>2</sub> solution (20.0 mM), 2.0 mL of H<sub>2</sub>PtCl<sub>6</sub> solution (19.3 mM), 0.7 mL of methanol, 602.6 mg of NaI, 200.0 mg of PVP, 303.4 mg of glycine were dissolved in a beaker and sonicated for 10.0 min, and stirred for another 12 h. The obtained solution was moved to a Teflon-lined autoclave. And then the mixture was heated to 200.0 °C and kept for 3 h. The final PtCuNi ic-NFs were obtained by centrifugation at 10000 rpm for 15.0 min, and continuous washed with a mixture of deionized water and ethanol. The synthetic recipe of PtCuNi echelon NFs (PtCuNi ie-NFs) is almost the same with that of PtCuNi ic-NFs except the n-propanol (0.7 mL) instead of methanol. In comparison with PtCuNi ic-NFs, the synthetic recipe for PtCuNi heliciform NFs (PtCuNi ih-NFs) has been changed, including altering the reaction time to 30 min, using 1,3-propanediol (0.7 mL) instead of methanol, and microwave heating instead of oven heating.

## **2.2 Characterization of PtCuNi NFs**

The external and internal structure of trimetallic PtCuNi NFs were measured by JEM 2100 transmission electron microscope (TEM). The EDX elemental mapping and high angle annular dark-field imaging-scanning transmission electron microscopy (HAADF-STEM) images were detected by Tecnai F20 TEM. X-ray diffraction patterns (XRD) of these PtCuNi

NFs were conducted on a powder X-ray diffractometer equipped with a Cu radiation source ( $\lambda = 0.15406$  nm). The loadings of the elements in PtCuNi NFs were detected by inductively coupled plasma-optical emission spectrometry (ICP-OES). X-ray photoelectron spectroscopy (XPS) analysis of PtCuNi NFs was performed on a PHI5000 Versaprobe system.

### **2.3 Electrochemical measurements**

The measurements of MOR and FAOR on these PtCuNi NFs were finished on a CHI 760e electrochemical analyzer (CHI Instrument, CHN). Before the measurements, all these samples were reduced by hydrogen at 250 °C for 30 min. The Pt sheet, catalyst modified glassy carbon electrode (GCE, 3 mm in diameter) and saturated calomel electrode (SCE) were selected as the counter, working and reference electrode, respectively. Before the measurements, a GCE was continuously polished with 0.3 and 0.05  $\mu\text{m}$   $\text{Al}_2\text{O}_3$  powders, respectively. Then, 6  $\mu\text{L}$  of ethanol and water solution (ethanol/water = 1/1 volume ratio) containing 6  $\mu\text{g}$  of PtCuNi NFs was dropped onto the surface of the prepared catalysts, and finally covered by 2  $\mu\text{L}$  of 0.05 wt% Nafion (Alfa Aesar).

The MOR (or FAOR) of these samples was carried out in a solution of 2 M  $\text{CH}_3\text{OH}$  (or 0.25 M  $\text{HCOOH}$ ) in 0.5 M  $\text{H}_2\text{SO}_4$  ( $\text{N}_2$ -saturated). The cyclic voltammetry (CV) measurements were carried out under the temperature of 25 °C, and the potential was scanned with the range from  $-0.24$  to  $1.0$  V (vs SCE) at a sweep rate of  $50$   $\text{mV s}^{-1}$ . The electrochemical surface areas (ECSA) of these PtCuNi NFs were obtained by using the hydrogen underpotential adsorption/desorption method. With regard to CO stripping tests, the GCE covered with PtCuNi NFs was first immersed in a CO-saturated 0.5 mol/L  $\text{H}_2\text{SO}_4$  aqueous solution for a certain time. Then, the CO species in the solution without adsorbed on the catalyst surface

was removed by bubbling the GCE with  $N_2$  for 10 min. Stripping measurements of PtCuNi NFs were conducted with the potential scanned from  $-0.24$  to  $1.0$  V (vs SCE) at the scan rate of  $50$   $mV\ s^{-1}$ .

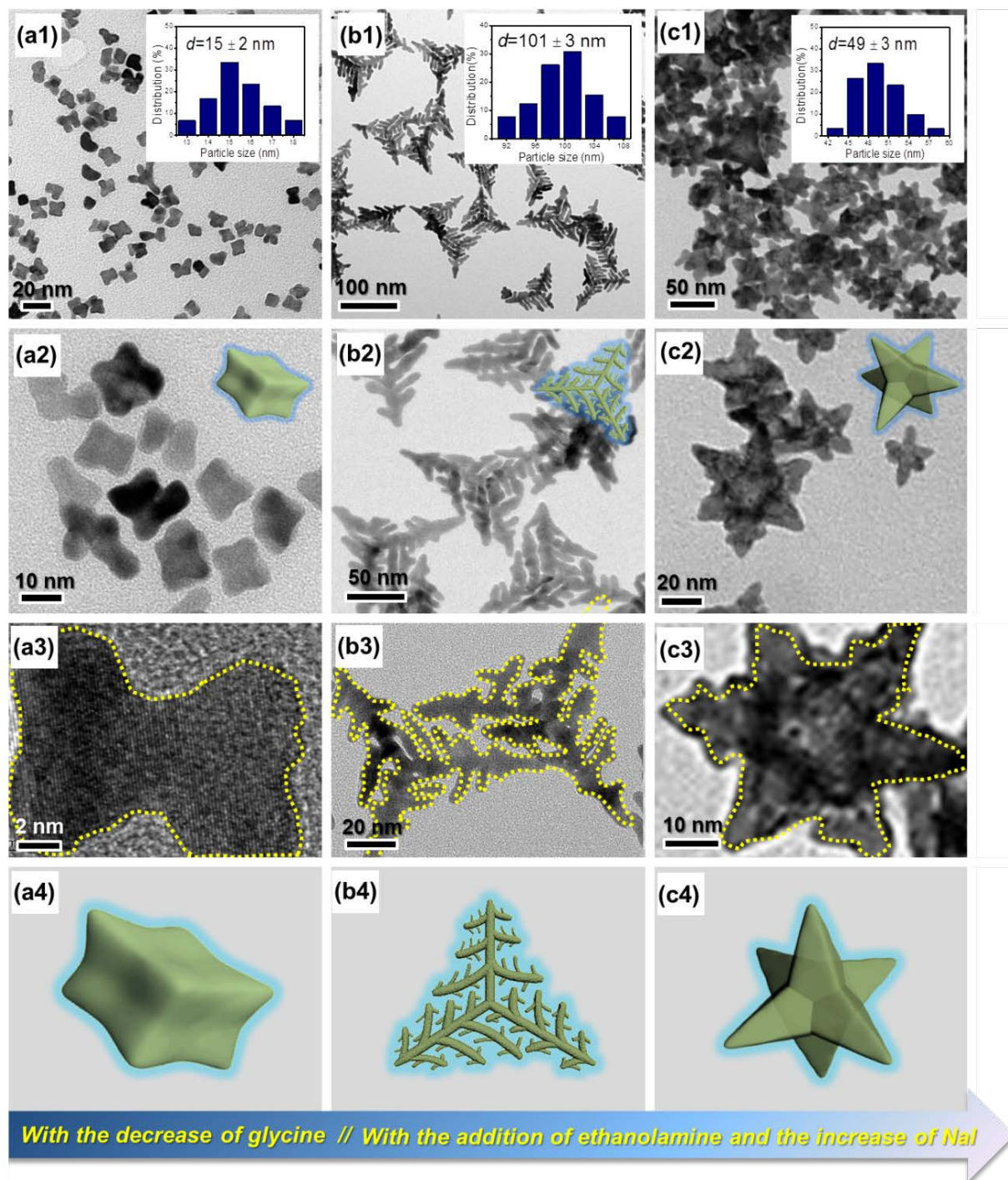


**Figure 1.** The TEM images, size frequency histograms (insert) and the corresponding 3D models of (a1-a4) PtCuNi ec-NFs, (b1-b4) PtCuNi eb-NFs, and (c1-c4) PtCuNi eh-NFs.

### **3 Results and discussion**

A one-pot reduction method was applied to fabricate PtCuNi NFs with tunable structure in the external and internal surface. In the synthesis process, copper chloride, nickel chloride and chloroplatinic acid were selected as the metal precursors, glycine, alcohol and NaI as the reducing agent and structure-directing agent, and deionized water as the solvent, respectively. The synthetic condition in this system was investigated to determine the important parameter in controlling the external and internal structure of PtCuNi NFs. Significantly, in this system, alcohol species were demonstrated to play the dominant role in governing the internal structure of PtCuNi NFs, while the glycine and NaI species were clarified as the main factors in controlling the external architecture of PtCuNi NFs. The optimized external and internal structure of PtCuNi NFs, combined a large amount of defects (e.g. vacancy, subtle lattice distortion and high-index facets), provides abundant coordinatively unsaturated sites for the efficient MOR and FAOR.

#### **3.1 Characterization of PtCuNi NFs with tunable external structures**

The morphologies of PtCuNi NFs with tunable external structures were characterized by TEM, and the representative images and the size distribution histograms are listed in Figure 1. The PtCuNi concave NFs (ec-NFs) in Figure 1(a1-a3) present a clear external concave structure, along with structure selectivity more than 90% and a face-to-face size of 15 nm. The pony-size PtCuNi ec-NFs can possess abundant active centers on the surface due to the high surface/volume ratio, which can enhance the utilization efficiency of Pt atoms. With the decreasing of the glycine amount from 303.4 to 100.0 mg and keeping other parameters identical, the external structure of PtCuNi NFs evolves from concave to branch (Figure

1(b1-b3)). The PtCuNi branch NFs (PtCuNi eb-NFs) exhibit a multihierarchical structure with a branch diameter of 8 nm, which can be in favor of the molecular reactant to contact the catalysts. In comparison with small nanoparticle materials, the eb-NFs improve the structure stability ascribed to the interconnection of the branches. Interestingly, PtCuNi hexapod NFs (PtCuNi eh-NFs, in Figure 1(c1-c3)) can be obtained when the NaI amount was increased to 602.6 mg, and the ethanolamine instead of ethylene glycol was used. The average particle diameter measured by apex-to-apex on a single eh-NF particle is about 49 nm. Noteworthy, the surface of PtCuNi eh-NFs is rough and contains many small gullies and protrusions, contributing to the formation of more active sites.

To further shed light on the external atomic arrangement of PtCuNi NFs, the HRTEM and HAADF-STEM characterization were performed (Figure 2 and Figure S1-S2). As observed (Figure 2(a-c)), the external surfaces of PtCuNi NFs samples are composed of abundant defects derived from the atomic vacancies, step atoms and/or high-index facets, which have been identified as the main active sites for the electro-oxidation of liquid fuels. HRTEM image presents that the PtCuNi ec-NFs, eb-NFs, and eh-NFs have an adjacent atom–atom distance of 0.216 nm (Figure S1), 0.217 nm (Figure 2) and 0.217 nm (Figure S2), respectively, which locates among the (111) plane of Pt (0.227 nm), Ni (0.203 nm) and Cu (0.209 nm), demonstrating the alloy structure of PtCuNi<sup>32-35</sup>. The HAADF-STEM micrographs and corresponding EDS elemental mapping analysis (Figure 2(d-k)) clarify that the Pt, Cu and Ni elements are evenly located on the whole structure, further demonstrating the alloy phase of PtCuNi NFs. Moreover, the HRTEM images (Figure 2(a-c) and Figure S1) reveal that lattice fringes of PtCuNi eb-NFs and ec-NFs continuously cover the whole particle with the absence of any stacking faults, illuminating the presence of single crystal structures. The molar ratio of

Cu/Pt/Ni for ec-NFs, eb-NFs, and eh-NFs detected by ICP-OES is 23.2/76.5/0.3, 23.4/76.0/0.6, and 22.3/76.3/1.4, respectively.

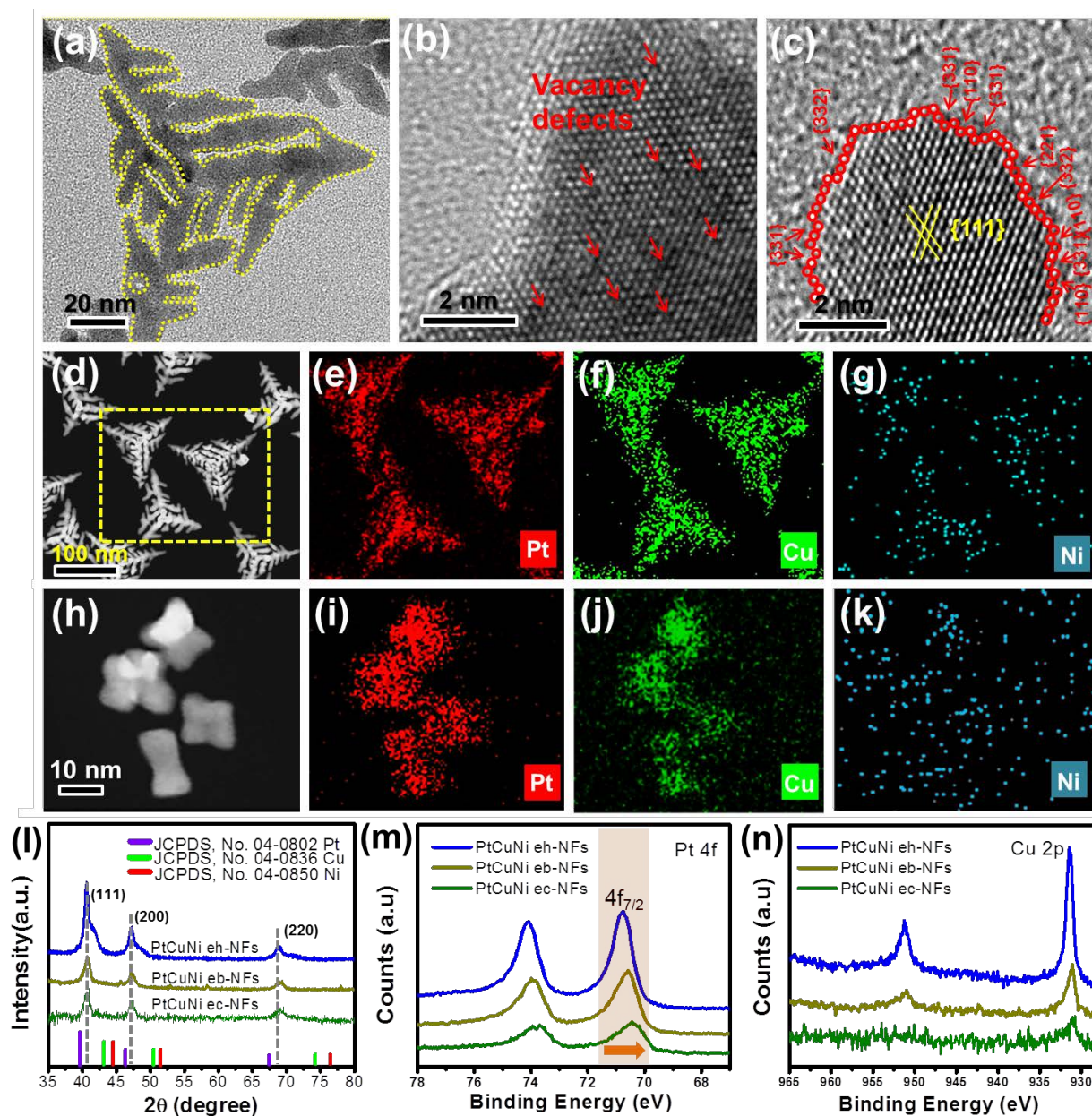


**Figure 2.** (a) TEM, (b) atomic vacancies, and (c) high-index facet micrographs of PtCuNi eb-NFs. HAADF-STEM micrographs and corresponding EDS mapping analysis of (d-g) PtCuNi eb-NFs and (h-k) PtCuNi ec-NFs. (l) The XRD patterns and (m & n) XPS spectra of PtCuNi alloys with different external structures.

XRD patterns (Figure 2l) of PtCuNi NFs with different external structures exhibit the characteristic peaks of the face-centered cubic (fcc) Pt, without the typical peaks of Ni and/or Cu metal, demonstrating the formation of PtCuNi alloy<sup>36, 37</sup>, consistent with the results of HRTEM and EDS-mapping. In comparison with the plane of pure Pt, the diffraction peaks of ec-NFs, eb-NFs, and eh-NFs shift to the higher values of 40.74°, 40.68°, and 40.61°, respectively, indicating a contraction of the lattice after the partial substitution of Pt atoms by smaller Ni and Cu atoms. Moreover, the asymmetrical peaks around 40° with regards to PtCuNi eh-NFs can be assigned to its heterogeneous composition, which results from the co-existence of galvanic replacement and co-reduction reactions during the alloying process. The XPS was used to further analyze the external surface composition and valence state of PtCuNi NFs. As observed from Figure 2m, the PtCuNi NFs with tunable external structures possess the binding energies of Pt(0) 4f<sub>7/2</sub> at 70.45-70.77 eV, transferring to lower energies relative to pure metallic Pt (70.90 eV). According to previous research<sup>38</sup>, these negative shifts of the Pt 4f<sub>7/2</sub> binding energies of PtCuNi NFs are relative to the electron donation from Cu and Ni to Pt. In parallel, the binding energies (Figure 2n) of Cu(0) 2p<sub>3/2</sub> of PtCuNi NFs transfer to higher energies compared with that of pure Cu (932.4 eV). The shift of the binding energy of the metal core level can result in the change of its d-band center relative to Fermi level<sup>39-41</sup>. An upshift of d-band center induced by electronic interactions between different metals can result in stronger adsorption energy, on the contrary, a downshift of d-band center leads to a lower one<sup>42</sup>. Thus, the optimization of d-band center of these elements in PtCuNi NFs can improve their electrocatalytic performance of MOR and FAOR.

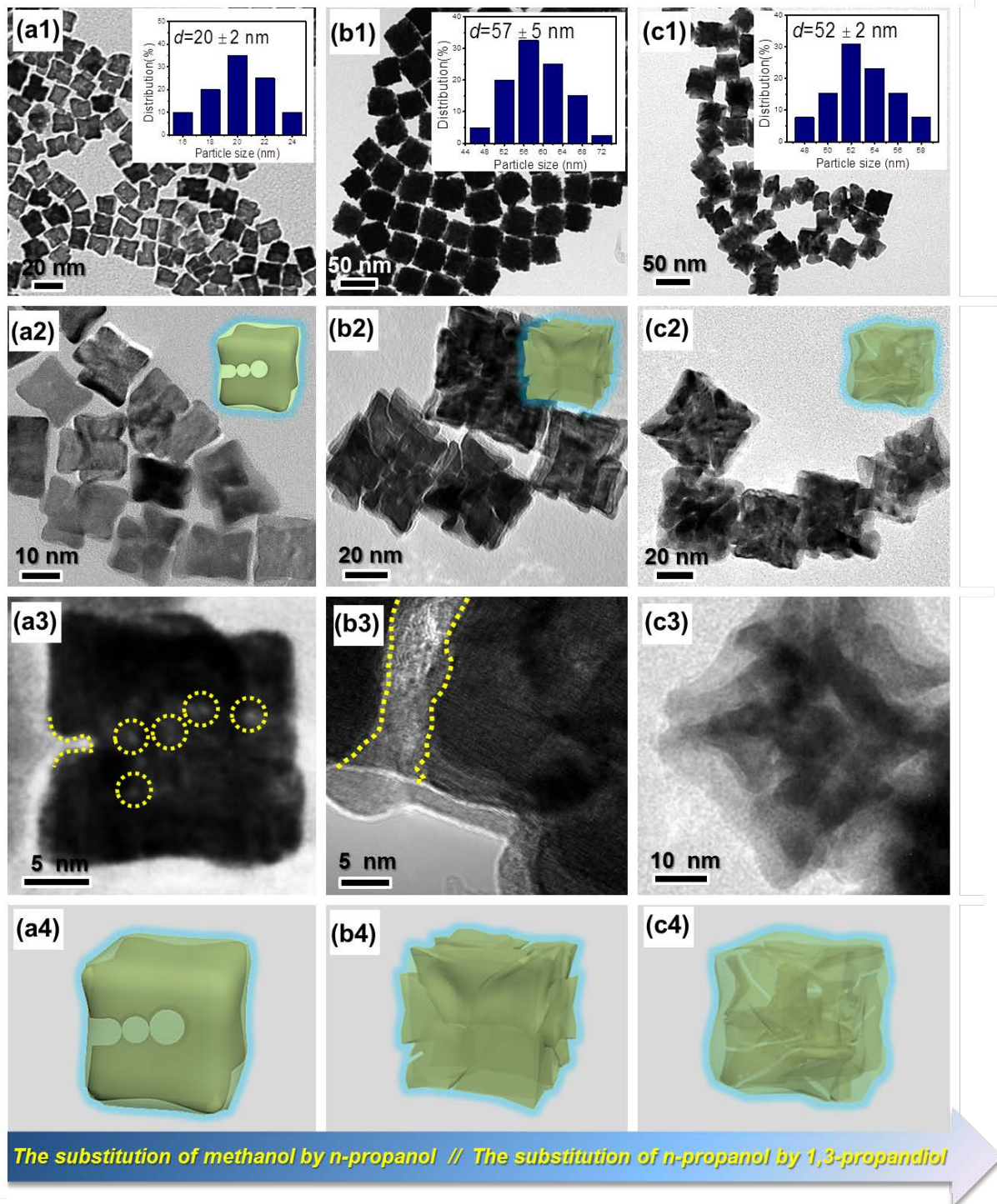


**Figure 3.** The TEM images, size frequency histograms (insert) and the corresponding 3D models of (a1-a4) PtCuNi ic-NFs, (b1-b4) PtCuNi ie-NFs, and (c1-c4) PtCuNi ih-NFs.

### 3.2 Characterization of PtCuNi NFs with tunable internal structures

The internal structures of PtCuNi NFs is of equal significance to the external structures due to

the exposure of the inside Pt active sites to contact with the reactants. The TEM (Figure 3) and HRTEM (Figure 4 and Figure S3-S4) present the detailed internal architecture of the PtCuNi NFs. The PtCuNi cavity NFs (PtCuNi ic-NFs) listed in Figure 3(a1-a3) possess a cavity in the center of the particle along with several mesochannels connecting to the external surface. The ic-NFs possess a high shape selectivity of approximate 95% and average apex-to-apex dimension of 20 nm. The PtCuNi echelon NFs (PtCuNi ie-NFs) were obtained when the methanol was substituted by n-propanol during the synthetic process. In comparison with ic-NFs, more interlaced mesochannels are formed and thread the inside of ie-NFs (Figure 3(b1-b3)). The internal structure of PtCuNi NFs evolves from echelon to heliciform by changing the n-propanol into 1,3-propanediol. The PtCuNi heliciform NFs (PtCuNi ih-NFs) exhibit 3-dimensional heliciform structure in the internal ih-NFs with an average size of 52 nm (Figure 3(c1-c3)). Moreover, as observed from the HRTEM images (Figure 4(a-c)), the internal surfaces of PtCuNi NFs consist of plenty of defects derived from the step atoms, atomic vacancies and interfacial dislocation. HRTEM images presents that the PtCuNi NFs with tunable internal structures have lattice spacing from 0.216 nm to 0.219 nm, which locates among the (111) planes of fcc Pt (0.227 nm), Ni (0.203 nm), and Cu (0.209 nm), demonstrating the solid-solution phase of PtCuNi NFs with tunable internal surface. The HAADF-STEM micrographs and corresponding EDS elemental mapping analysis (Figure 4(d-k) and Figure S3(c-f)) reveal that the Pt, Cu and Ni elements are uniformly located on entire framework, further certifying the alloy phase of PtCuNi NFs with different internal structures. The molar ratio of Cu/Pt/Ni for ic-NFs, ie-NFs, and ih-NFs detected by ICP-OES is 22.0/77.1/0.9, 31.0/54.1/14.9, and 17.1/80.6/2.3, respectively.

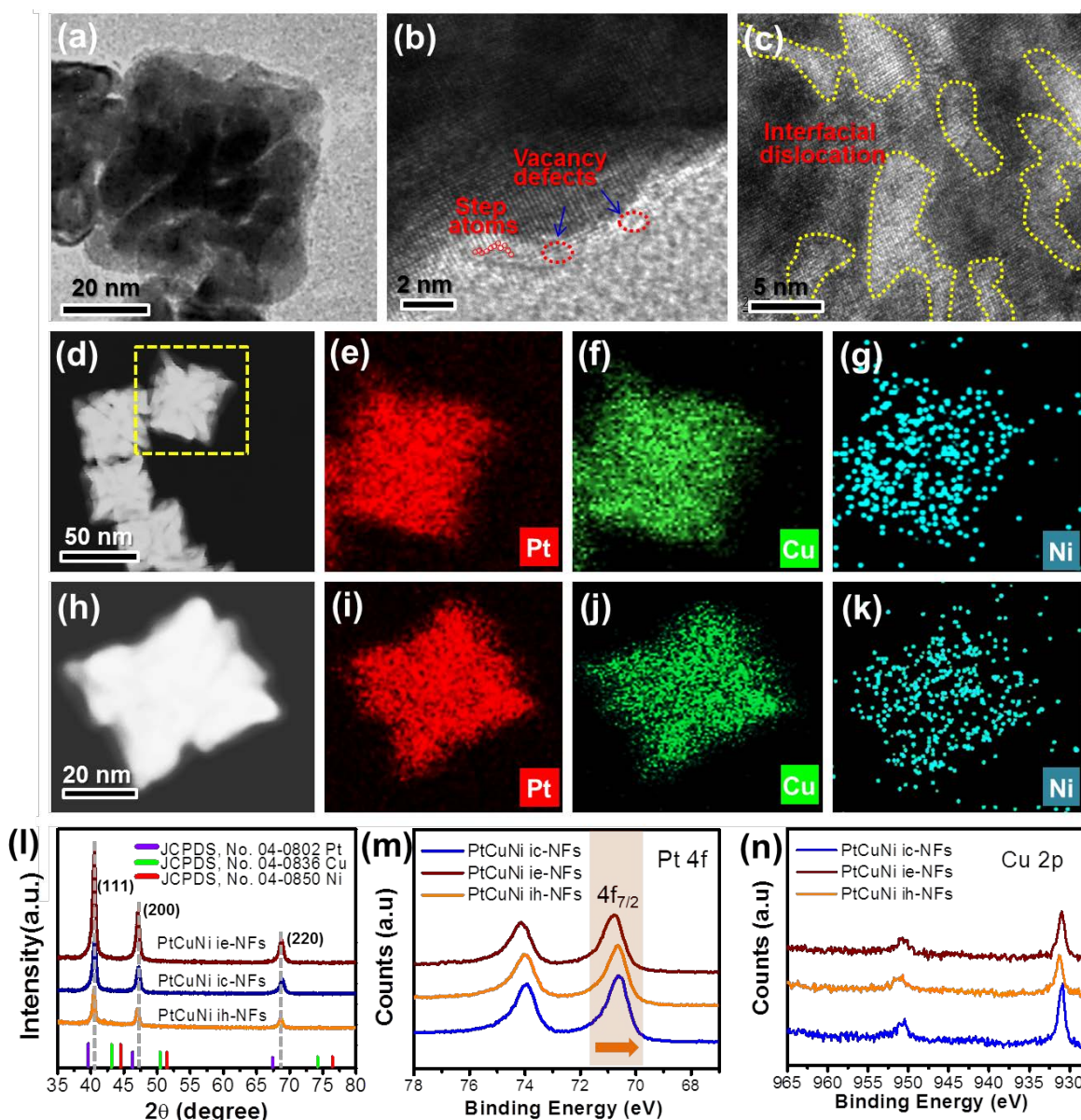


**Figure 4.** (a) TEM and (b and c) HRTEM micrographs of PtCuNi ih-NFs. HAADF-STEM micrographs and corresponding EDS mapping analysis of (d-g) PtCuNi ih-NFs and (h-k) PtCuNi ie-NFs. (l) The XRD patterns and (m & n) XPS spectra of PtCuNi NFs with different internal structures.

XRD patterns (Figure 4l) of PtCuNi NFs were obtained to further characterize the phase of PtCuNi NFs with tunable internal architecture. The diffraction peaks indexed to the (111), (200) and (220) planes of PtCuNi alloy are both located to the sites among the values of fcc Pt, Ni, and Cu, confirming the formation of PtCuNi alloy, consistent with the results of HRTEM

and EDS-mapping. The alloy phase and surface composition of the PtCuNi NFs with tunable internal architecture were further determined by XPS. The PtCuNi NFs with tunable internal structures show the binding energies of Pt(0) 4f<sub>7/2</sub> at 70.62-70.75 eV (Figure 4(m)), revealing the negative shift of the Pt 4f<sub>7/2</sub> peaks compared to that of pure metallic Pt (4f<sub>7/2</sub>: 70.90 eV)<sup>38, 43, 44</sup>. The negative shift of the Pt 4f<sub>7/2</sub> peaks is attributed to the optimized electronic structure of Pt after the implantation of Cu and Ni atoms. The binding energies (Figure 4(n)) of Cu(0) 2p<sub>3/2</sub> of PtCuNi NFs transfer to higher energies compared with that of pure Cu (932.4 eV). Moreover, the Ni 2p peak intensities for PtCuNi NFs are almost undetectable assigned to the low content of Ni in PtCuNi NFs.

Based on the above discussion, it can be concluded that the external and internal structures of PtCuNi NFs are mainly controlled by the alcohol, glycine and NaI species during the synthetic process. The n-propanol, 1,3-propanediol and methanol have a great effect on tailoring the internal structures of PtCuNi NFs, while the glycine and NaI species are the main factors in fabrication of unique external structure. To further study the formation mechanism of PtCuNi NFs with tunable interfacial structures, the interaction between the stabilizing and reducing agents and Pt(IV), Ni(II), and Cu(II) species were studied by UV-vis spectroscopy. It can be revealed that the Pt (IV) ions have a strong coordination with ethanolamine and NaI species, while exhibit nearly no interaction with glycine, n-propanol, 1,3-propanediol, ethylene glycol and methanol (Figure 5 and Figure S5-S9). The Cu (II) ions have obviously coordination with glycine, ethanolamine, NaI and ethylene glycol species, while possess weak interaction with n-propanol, 1,3-propanediol and methanol. Additionally, as observed from the UV-vis spectra results, the Ni (II) ions almost have no coordination with all the above reagents except ethylene glycol. Moreover, I<sup>-</sup> ions can selectively adsorb on the (100) facets

of Pt and alter their atomic addition on the surface facets, and further affect the final structure of PtCuNi NFs. Taken together, these coordinating and/or structure-directing agents can control the nucleation/growth kinetics of trimetallic PtCuNi NFs, which further result in the variable external and internal structures.

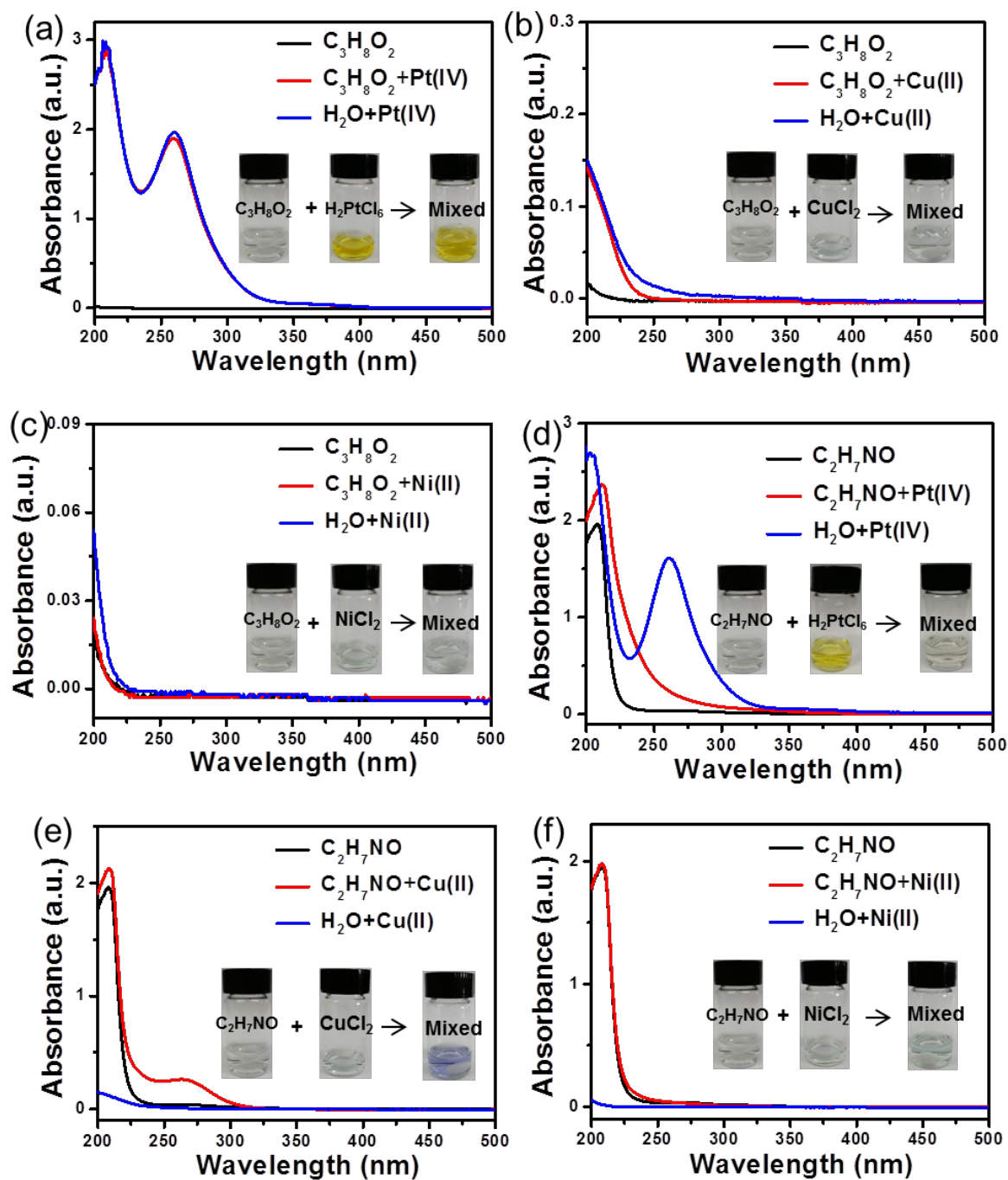


**Figure 5.** In-situ UV-vis spectroscopy studies of the interaction between (a-c) 1,3-propanediol and (d-f) ethanolamine and Pt(IV), Cu(II) and Ni(II) ions.

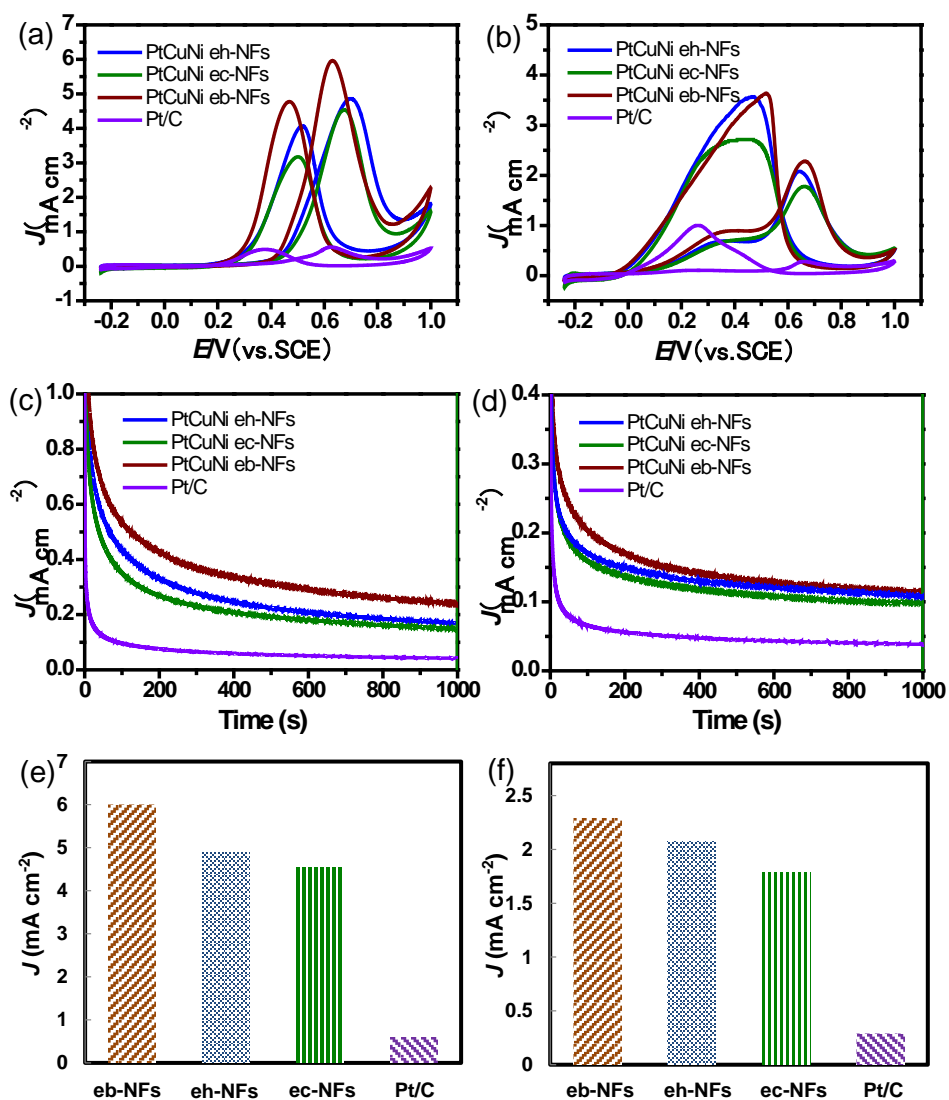


**Figure 6** Cyclic voltammogram (CV) curves of (a) methanol and (b) formic acid electrooxidation over PtCuNi NFs with different external surface and Pt/C.  $i-t$  curves of these catalysts for (c) methanol (at 0.4 V) and (d) formic acid (at 0.06 V) electrooxidation. Specific activities of (e) MOR and (f) FAOR calculated by  $J$  normalized to the ECSA.

### 3.3 Catalytic performance for electro-oxidation of liquid fuels

MOR and FAOR were used as the probe reactions to investigate the surface structure and defect effects on the electrocatalytic performance of the as-synthesized PtCuNi NFs as well as commercial Pt/C catalyst. Figure 6a displays the cyclic voltammograms of methanol oxidation of the eh-NFs, ec-NFs and eb-NFs PtCuNi alloy with different external structures. The specific current density ( $J$ ) was normalized to the ECSA obtained from the hydrogen

adsorption/desorption method (Figure S10)<sup>11, 45</sup>. The peak current densities for MOR in the positive potential scan for eh-NFs, ec-NFs, eb-NFs PtCuNi, and commercial Pt/C were 4.89, 4.53, 6.01, and 0.56 mA/cm<sup>2</sup>, respectively. The eb-NFs showed higher specific activity than other samples, which can be assigned to their unique geometry associated with high defect-density. The oxidation current density in the positive potential of eb-NFs is approximately 10.7 times bigger than that of Pt/C. The electrocatalytic retention of PtCuNi catalysts with different external structures was measured by chronoamperometry curves. As listed in Figure 6c, the activity retention of PtCuNi catalysts follows the order of PtCuNi eb-NFs > PtCuNi eh-NFs > PtCuNi ec-NFs > Pt/C. Additionally, we also found the activity enhancement of PtCuNi NFs with tunable external structures for formic acid electrooxidation relative to the benchmark Pt/C. These catalytic results (Figure 6b, 6d and 6f) of formic acid electrooxidation are consistent with those of MOR. The excellent electrocatalytic activity of PtCuNi eb-NFs for both oxidation reactions can be attributed to the abundant coordinatively unsaturated sites derived from high-index facets and vacancy defects in the external surface.

In parallel, the PtCuNi NFs with variable internal structures were also evaluated by MOR and FAOR. Figure 7a compares the intrinsic activities of various catalysts for MOR, shows an activity trend of PtCuNi ih-NFs > PtCuNi ie-NFs > PtCuNi ic-NFs > Pt/C, in line with the observation of anodic peak current density. Notably, the PtCuNi ih-NFs show more than 7.0 times of magnitude increase in specific activity compared with commercial Pt/C. We also assessed the electrocatalytic stability for MOR by means of chronoamperometry test. As observed (Figure 7c), the activity retention of PtCuNi catalysts follows the order of PtCuNi ih-NFs > PtCuNi ie-NFs > PtCuNi ic-NFs > Pt/C. Additionally, we also found activity enhancement of our PtCuNi NFs with variable internal structures for formic acid electrooxidation relative to the benchmark Pt/C (Figure 7b, 7d and 7f). The excellent activity

of PtCuNi ih-NFs for both electrooxidation reactions can be attributed to the abundant coordinatively unsaturated sites, including step vacancy defects, intragranular and interfacial dislocation in the internal surface. For comparison, the bimetallic PtCu and PtNi alloys (Figure S11) were also synthesized and evaluated in this study. The PtCu and PtNi alloys both exhibit insufficient activities compared to PtCuNi NFs (Figure S12), clarifying that the Cu and Ni atoms in trimetallic PtCuNi NFs can synergistically optimize the electronic structure of PtCuNi and further boost their performances of MOR and FAOR.

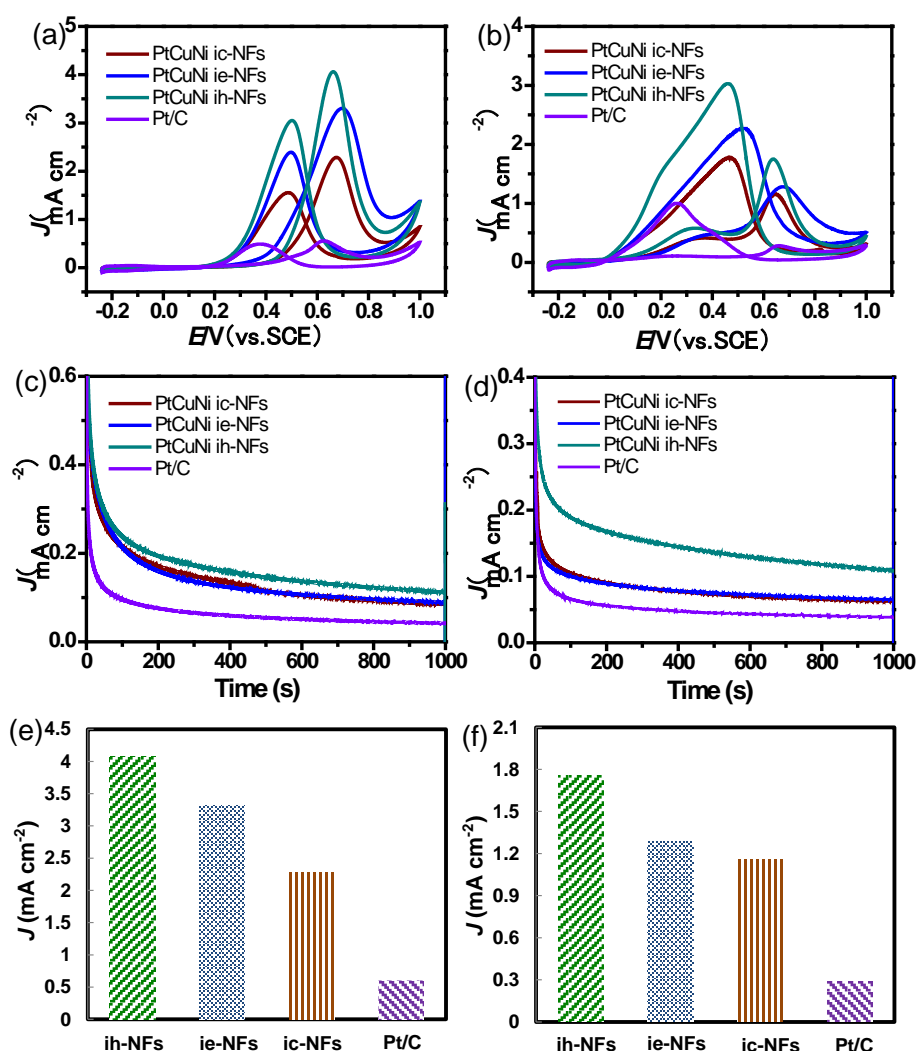


**Figure 7** Cyclic voltammogram (CV) curves of (a) methanol and (b) formic acid electrooxidation over PtCuNi NFs with different internal surface and Pt/C.  $i-t$  curves of these catalysts for (c) methanol (at 0.4 V) and (d) formic acid (at 0.06 V) electrooxidation. Specific activities of (e) MOR and (f) FAOR calculated by  $J$  normalized to the ECSA.

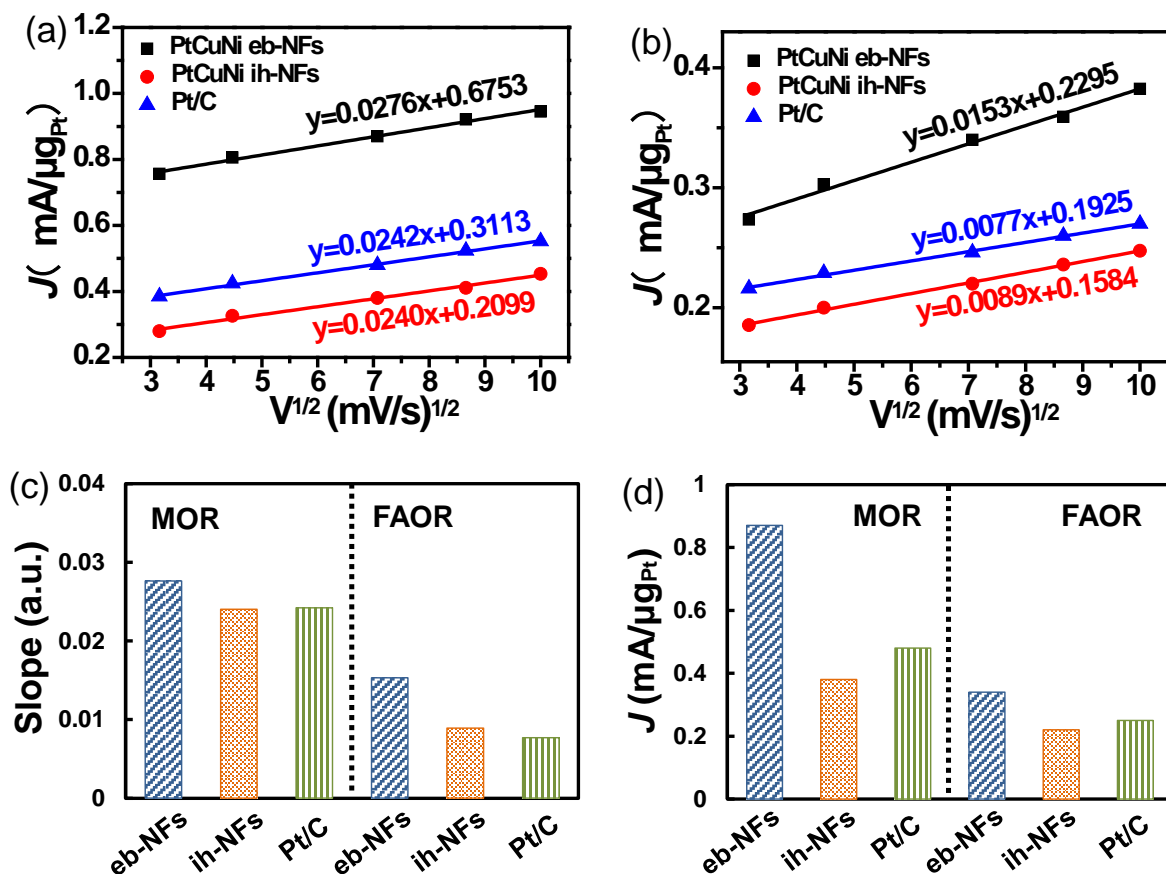


**Figure 8** The plots of mass activity  $J$  (mA/ $\mu\text{g}_{\text{Pt}}$ ) versus the square root of the scan rate ( $v^{1/2}$ ) for (a) MOR and (b) FAOR. (c) The slope histogram of eb-NFs, ih-NFs and Pt/C obtained from the fitting of  $J$  versus  $v^{1/2}$ . (d) The mass activity histogram of eb-NFs, ih-NFs and Pt/C for MOR and FAOR with the scan rate of 50 mV/s.

The electrooxidation kinetics of methanol and formic acid over the as-synthesized PtCuNi NFs with different internal and external structures were measured by an accelerated durability test. Different scan rates changing from 10 to 100 mV s $^{-1}$  during CV measurement were conducted. Figure 8a and 8b present the plots of the mass activity (mA/ $\mu\text{g}_{\text{Pt}}$ ) versus the square root of the scan rate (mV/s) $^{1/2}$ . As observed from Figure 8, the square root of the scan rate presents linear relationship with the mass activity, which clarifies that the MOR and FAOR on these catalysts follow the diffusion controlled process. The slope values of PtCuNi eb-NFs,

PtCuNi ih-NFs and Pt/C for MOR (FAOR) are 0.0276 (0.0153), 0.0240 (0.0089), and 0.0242 (0.0077), respectively. The higher slope value of the PtCuNi eb-NFs in comparison with those of PtCuNi ih-NFs and Pt/C demonstrates the enhancement of methanol and formic acid diffusion rates on PtCuNi eb-NFs<sup>46,47</sup>. The excellent diffusion ability of PtCuNi eb-NFs for MOR and FAOR can be attributed to the optimized surface structures along with plentiful external surface area.

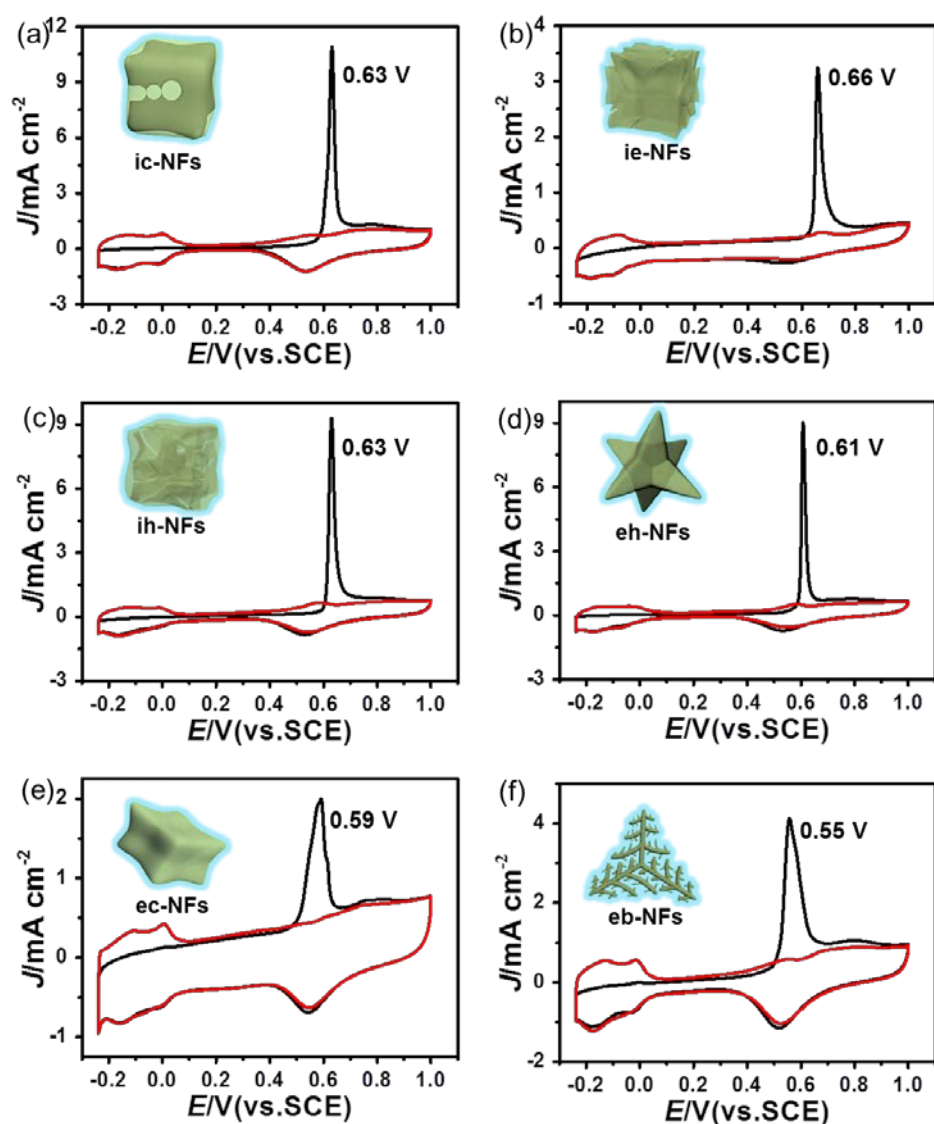
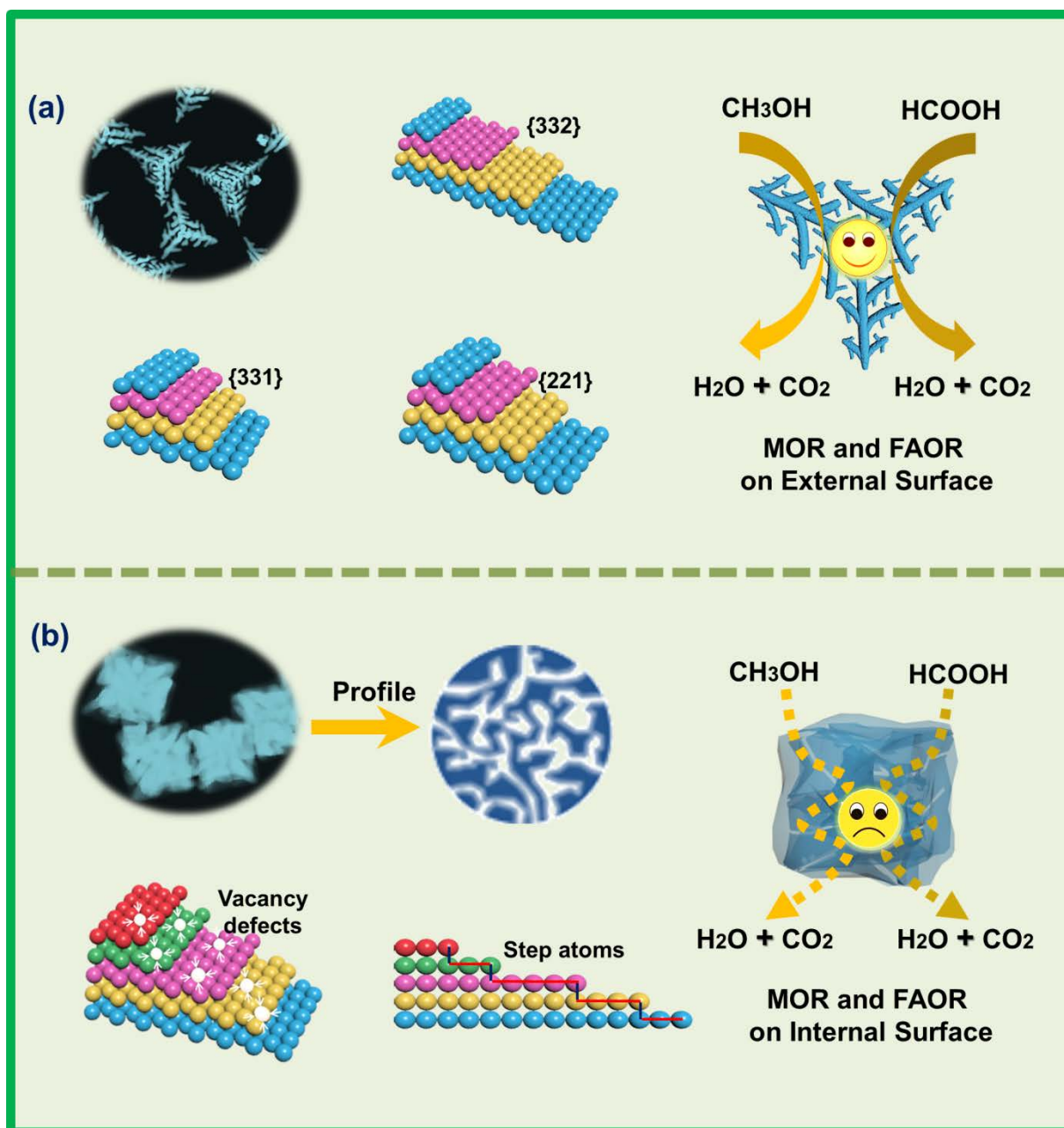


**Figure 9** CO-stripping voltammogram curves of (a) PtCuNi ic-NFs, (b) PtCuNi ie-NFs, (c) PtCuNi ih-NFs, (d) PtCuNi eh-NFs, (e) PtCuNi ec-NFs and (f) PtCuNi eb-NFs.

To further investigate the poisoning resistance of PtCuNi NFs during MOR and FAOR processes, CO-stripping experiments were carried out. As previously demonstrated<sup>48-51</sup>, Pt-CO<sub>ads</sub> is a poisoning intermediate and hinders the reaction processes of methanol and formic acid electrooxidation. The adsorbed CO<sub>ads</sub> molecules are difficult to be eliminated unless the OH<sub>ads</sub> species was generated on the surface of catalyst. As observed from the CO-stripping results (Figure 9), it is revealed that the adsorbed CO<sub>ads</sub> species on PtCuNi surface is completely oxidized in the first CV cycle. According to the poisoning resistance studies in MOR and FAOR, the Pt surface imbedded with an oxophilic metal adsorbs hydroxyl groups (OH<sub>ads</sub>) at lower potential than that of pure Pt surface<sup>31, 36</sup>. Fortunately, the additional Cu and Ni atoms in the PtCuNi alloy surface can adsorb OH<sub>ads</sub> species at a lower potential, serving as the oxidant to efficiently eliminate the CO<sub>ads</sub> species. As observed in Figure 9 and Table S1, the peak potentials of CO<sub>ads</sub> oxidation over PtCuNi NFs present a down-shift relative to commercial Pt/C, clarifying the improved CO anti-poisoning property on PtCuNi NFs. Specifically, among these catalysts, the PtCuNi eb-NFs show the largest down-shift (peak potential 0.55 V). Noteworthy, the PtCuNi NFs with variable external structures exhibited better anti-CO-poisoning capability than PtCuNi NFs with tunable internal surface structures, which can be attributed to the faster diffusion rate and decreased readsorption of CO species in the external surface.



**Scheme 2.** Schematic illustration of the surface structure model, MOR and FAOR processes over (a) PtCuNi eb-NFs and (b) PtCuNi ih-NFs.

### 3.4 Structure-activity relationship

Based on the above discussion, it is concluded that the PtCuNi NFs with variable external structures possess higher performance (activity and anti-CO-poisoning capability) than those with tunable internal structures as well as commercial Pt/C, which can be assigned to the following points (Scheme 2). First, the PtCuNi NFs with plentiful external surface area endow

excellent diffusion rate of poisonous species to the solution phase, which can restrain the adsorption of poisonous molecules (such as CO) on PtCuNi NFs surface. Compared with PtCuNi NFs with affluent external surface, PtCuNi NFs with abundant internal surface area exhibit poor diffusion rate of reaction molecules (such as the CO species in the internal mesochannels), resulting in their lower CO anti-poisoning ability, consistent with the CO stripping measurement results. Second, the introduction of Cu and Ni atoms into the Pt lattice can optimize the electronic structure of PtCuNi NFs, which can decrease the adsorption probability of poisonous species (such as CO molecule) on PtCuNi NFs and thus improve their MOR and FAOR activities. Third, the PtCuNi alloys with nanoframe morphology possess three-dimension structure, which can increase their surface area and provide plentiful catalytic sites to reactant species. Finally, the PtCuNi NFs with high density of vacancy, high-index facets and subtle lattice distortion can contribute to the formation of more coordinatively unsaturated sites (defects). These defects are considered as the main catalytic sites for MOR and FAOR, especially for the enhanced OH adsorption ability, further boosting their resistance to CO poison. Therefore, the external surface-constructed PtCuNi NFs with high defect-density (such as PtCuNi eb-NFs) are proposed as the excellent electrocatalysts for MOR and FAOR applications.

#### **4 Conclusion**

Three-dimensional PtCuNi NFs with tunable external- and internal-surface structures were successfully synthesized by a one-pot wet-chemical reduction approach. Alcohol species were clarified to play the dominant role in governing the internal structure of PtCuNi NFs, while the glycine and NaI species were demonstrated as the main factors in controlling the external architecture of PtCuNi NFs. The optimized external structure of PtCuNi NFs, combining with

a large amount of defects and high-index facets, provides abundant catalytic sites and excellent diffusion rate for the MOR and FAOR. The catalytic results showed that the PtCuNi eb-NFs with plentiful external surface area exhibit higher anti-CO-poisoning capability and better specific activity than those with tunable internal structures as well as commercial Pt/C. Thus, our work suggests that the electrooxidation performance (anti-poisoning property and diffusion rate) is best enhanced by increasing the external rather than the internal surface area. This insight is important for improving the synthesis of future catalysts.

### **Associated content**

The supplemental information is available free of charge on the ACS Publications website at <http://pubs.acs.org>. Detailed description of reagents and chemicals, TEM images, in-situ UV-vis spectroscopy and CO-stripping experiment results.

### **Corresponding author**

\*E-mail, [chm\\_lics@ujn.edu.cn](mailto:chm_lics@ujn.edu.cn).

\*E-mail, [chm\\_chengz@ujn.edu.cn](mailto:chm_chengz@ujn.edu.cn).

### **Notes**

The authors declare no competing financial interest.

### **Acknowledgements**

This work was supported by the Key Research and Development Program of Shandong Province (No. 2019GSF109115), National Natural Science Foundation of China (No. 21808079, 21908174 and 21878121), Shandong Provincial Natural Science Foundation (No. ZR2017BB029 and ZR2018MB004), China Postdoctoral Science Foundation (No. 2017M610405), National Postdoctoral Program for Innovative Talents from China (No.

BX20190280), International Postdoctoral Exchange Fellowship Program Between Helmholtz-Zentrum Berlin für Materialien und Energie GmbH, OCPC and University of Jinan.

## References

- (1) Aricò, A. S.; Srinivasan, S.; Antonucci, V. DMFCs: From Fundamental Aspects to Technology Development. *Fuel Cells* **2001**, *1*, 133-161.
- (2) Seh, Z. W.; Kibsgaard, J.; Dickens, C. F.; Chorkendorff, I.; Nørskov, J. K.; Jaramillo, T. F. Combining theory and experiment in electrocatalysis: Insights into materials design. *Science* **2017**, *355*.
- (3) Li, C. W.; Ciston, J.; Kanan, M. W. Electroreduction of carbon monoxide to liquid fuel on oxide-derived nanocrystalline copper. *Nature* **2014**, *508*, 504-507.
- (4) Yang, P.; Yuan, X.; Hu, H.; Liu, Y.; Zheng, H.; Yang, D.; Chen, L.; Cao, M.; Xu, Y.; Min, Y.; Li, Y.; Zhang, Q. Solvothermal Synthesis of Alloyed PtNi Colloidal Nanocrystal Clusters (CNCs) with Enhanced Catalytic Activity for Methanol Oxidation. *Adv. Funct. Mater.* **2018**, *28*, 1704774.
- (5) Luo, M.; Guo, S. Strain-controlled electrocatalysis on multimetallic nanomaterials. *Nat. Rev. Mater.* **2017**, *2*, 17059.
- (6) Tripković, D. V.; Popović, K. D.; Jovanović, V. M.; Nogueira, J. A.; Varela, H.; Lopes, P. P.; Strmcnik, D.; Stamenkovic, V. R.; Markovic, N. M. Tuning of catalytic properties for electrooxidation of small organic molecules on Pt-based thin films via controlled thermal treatment. *J. Catal.* **2019**, *371*, 96-105.
- (7) Anitha, V. C.; Zazpe, R.; Krbal, M.; Yoo, J.; Sopha, H.; Prikryl, J.; Cha, G.; Slang, S.; Schmuki, P.; Macak, J. M. Anodic TiO<sub>2</sub> nanotubes decorated by Pt nanoparticles using ALD:

An efficient electrocatalyst for methanol oxidation. *J. Catal.* **2018**, *365*, 86-93.

(8) Dao, D. V.; Adilbish, G.; Le, T. D.; Nguyen, T. T. D.; Lee, I.-H.; Yu, Y.-T. Au@CeO<sub>2</sub> nanoparticles supported Pt/C electrocatalyst to improve the removal of CO in methanol oxidation reaction. *J. Catal.* **2019**, *377*, 589-599.

(9) Du, H.; Luo, S.; Wang, K.; Tang, M.; Sriphathoorat, R.; Jin, Y.; Shen, P. K. High-Quality and Deeply Excavated Pt<sub>3</sub>Co Nanocubes as Efficient Catalysts for Liquid Fuel Electrooxidation. *Chem. Mater.* **2017**, *29*, 9613-9617.

(10) Xue, S.; Deng, W.; Yang, F.; Yang, J.; Amiin, I. S.; He, D.; Tang, H.; Mu, S. Hexapod PtRuCu Nanocrystalline Alloy for Highly Efficient and Stable Methanol Oxidation. *ACS Catal.* **2018**, *8*, 7578-7584.

(11) Ma, Y.; Yin, L.; Yang, T.; Huang, Q.; He, M.; Zhao, H.; Zhang, D.; Wang, M.; Tong, Z. One-Pot Synthesis of Concave Platinum–Cobalt Nanocrystals and Their Superior Catalytic Performances for Methanol Electrochemical Oxidation and Oxygen Electrochemical Reduction. *ACS Appl. Mater. Inter.* **2017**, *9*, 36164-36172.

(12) Huang, L.; Zhang, X.; Wang, Q.; Han, Y.; Fang, Y.; Dong, S. Shape-Control of Pt–Ru Nanocrystals: Tuning Surface Structure for Enhanced Electrocatalytic Methanol Oxidation. *J. Am. Chem. Soc.* **2018**, *140*, 1142-1147.

(13) Gilroy, K. D.; Ruditskiy, A.; Peng, H.-C.; Qin, D.; Xia, Y. Bimetallic Nanocrystals: Syntheses, Properties, and Applications. *Chem. Rev.* **2016**, *116*, 10414-10472.

(14) Guo, S.; Zhang, S.; Sun, S. Tuning nanoparticle catalysis for the oxygen reduction reaction. *Angew. Chem. Int. Ed.* **2013**, *52*, 8526-8544.

(15) Luo, M. C.; Sun, Y. J.; Zhang, X.; Qin, Y. N.; Li, M. Q.; Li, Y. J.; Li, C. J.; Yang, Y.; Wang, L.; Gao, P.; Lu, G.; Guo, S. J. Stable High-Index Faceted Pt Skin on Zigzag-Like PtFe

Nanowires Enhances Oxygen Reduction Catalysis. *Adv. Mater.* **2018**, *30*, 1705515.

(16) Jiang, K.; Zhao, D.; Guo, S.; Zhang, X.; Zhu, X.; Guo, J.; Lu, G.; Huang, X. Efficient oxygen reduction catalysis by subnanometer Pt alloy nanowires. *Sci. adv.* **2017**, *3*, e1601705.

(17) Huang, X.; Tang, S.; Mu, X.; Dai, Y.; Chen, G.; Zhou, Z.; Ruan, F.; Yang, Z.; Zheng, N. Freestanding palladium nanosheets with plasmonic and catalytic properties. *Nat. Nanotechnol.* **2011**, *6*, 28-32.

(18) Yang, N.; Zhang, Z.; Chen, B.; Huang, Y.; Chen, J.; Lai, Z.; Chen, Y.; Sindoro, M.; Wang, A. L.; Cheng, H.; Fan, Z.; Liu, X.; Li, B.; Zong, Y.; Gu, L.; Zhang, H. Synthesis of Ultrathin PdCu Alloy Nanosheets Used as a Highly Efficient Electrocatalyst for Formic Acid Oxidation. *Adv. Mater.* **2017**, *29*, 1700769.

(19) Huang, X.; Zhu, E.; Chen, Y.; Li, Y.; Chiu, C. Y.; Xu, Y.; Lin, Z.; Duan, X.; Huang, Y. A facile strategy to Pt<sub>3</sub>Ni nanocrystals with highly porous features as an enhanced oxygen reduction reaction catalyst. *Adv. Mater.* **2013**, *25*, 2974-9.

(20) Kim, D.-S.; Kim, C.; Kim, J.-K.; Kim, J.-H.; Chun, H.-H.; Lee, H.; Kim, Y.-T. Enhanced electrocatalytic performance due to anomalous compressive strain and superior electron retention properties of highly porous Pt nanoparticles. *J. Catal.* **2012**, *291*, 69-78.

(21) Chen, C.; Kang, Y.; Huo, Z.; Zhu, Z.; Huang, W.; Xin, H. L.; Snyder, J. D.; Li, D.; Herron, J. A.; Mavrikakis, M.; Chi, M.; More, K. L.; Li, Y.; Markovic, N. M.; Somorjai, G. A.; Yang, P.; Stamenkovic, V. R. Highly Crystalline Multimetallic Nanoframes with Three-Dimensional Electrocatalytic Surfaces. *Science* **2014**, *343*, 1339-1343.

(22) Huang, L.; Wei, M.; Hu, N.; Tsiakaras, P.; Kang Shen, P. Molybdenum-modified and vertex-reinforced quaternary hexapod nano-skeletons as efficient electrocatalysts for methanol oxidation and oxygen reduction reaction. *Appl. Catal. B* **2019**, *258*, 117974.

- (23) Gao, D. W.; Li, S. N.; Song, G. L.; Luo, M. C.; Lv, Y. P.; Yang, S. H.; Ma, X. L.; Zhang, X.; Li, C. C.; Wei, Q.; Chen, G. Z. Inner space- and architecture-controlled nanoframes for efficient electro-oxidation of liquid fuels. *J. Mater. Chem. A* **2019**, *7*, 19280-19289.
- (24) Wang, Z.; Huang, L.; Tian, Z. Q.; Shen, P. K. The controllable growth of PtCuRh rhombic dodecahedral nanoframes as efficient catalysts for alcohol electrochemical oxidation. *J. Mater. Chem. A* **2019**, *7*, 18619-18625.
- (25) Kwon, T.; Jun, M.; Kim, H. Y.; Oh, A.; Park, J.; Baik, H.; Joo, S. H.; Lee, K. Vertex-Reinforced PtCuCo Ternary Nanoframes as Efficient and Stable Electrocatalysts for the Oxygen Reduction Reaction and the Methanol Oxidation Reaction. *Adv. Funct. Mater.* **2018**, *28*, 1706440.
- (26) Gardeniers, H. J. G. E. Chemistry in nanochannel confinement. *Anal. Bioanal. Chem.* **2009**, *394*, 385-397.
- (27) Cárdenas, H.; Müller, E. A. Molecular Simulation of the Adsorption and Diffusion in Cylindrical Nanopores: Effect of Shape and Fluid-Solid Interactions. *Molecules* **2019**, *24*, 608.
- (28) Hassan, H. B.; Rahim, A.; Khalil, M.; Mohammed, R. Ni Modified MCM-41 as a Catalyst for Direct Methanol Fuel Cells. *Int. J. Electrochem. Sci.* **2014**, *9*, 760-777.
- (29) Chu, Y.; Li, G.; Huang, L.; Yi, X.; Xia, H.; Zheng, A.; Deng, F., External or internal surface of H-ZSM-5 zeolite, which is more effective for the Beckmann rearrangement reaction? *Catal. Sci. Technol.* **2017**, *7*, 2512-2523.
- (30) Qi, Y.; Bian, T.; Choi, S.-I.; Jiang, Y.; Jin, C.; Fu, M.; Zhang, H.; Yang, D. Kinetically controlled synthesis of Pt-Cu alloy concave nanocubes with high-index facets for methanol electro-oxidation. *Chem. Commun.* **2014**, *50*, 560-562.

- (31) Gao, D.; Li, S.; Lv, Y.; Zhuo, H.; Zhao, S.; Song, L.; Yang, S.; Qin, Y.; Li, C.; Wei, Q.; Chen, G. PtNi colloidal nanoparticle clusters: Tuning electronic structure and boundary density of nanocrystal subunits for enhanced electrocatalytic properties. *J. Catal.* **2019**, *376*, 87-100.
- (32) Kuang, Y.; Zhang, Y.; Cai, Z.; Feng, G.; Jiang, Y.; Jin, C.; Luo, J.; Sun, X. Single-crystalline dendritic bimetallic and multimetallic nanocubes. *Chem. Sci.* **2015**, *6*, 7122-7129.
- (33) Gao, D.; Li, S.; Song, G.; Zha, P.; Li, C.; Wei, Q.; Lv, Y.; Chen, G. One-pot synthesis of Pt-Cu bimetallic nanocrystals with different structures and their enhanced electrocatalytic properties. *Nano Res.* **2018**, *11*, 2612-2624.
- (34) Xu, X.; Zhang, X.; Sun, H.; Yang, Y.; Dai, X.; Gao, J.; Li, X.; Zhang, P.; Wang, H.-H.; Yu, N.-F.; Sun, S.-G. Synthesis of Pt–Ni Alloy Nanocrystals with High-Index Facets and Enhanced Electrocatalytic Properties. *Angew. Chem. Int. Ed.* **2014**, *126*, 12730-12735.
- (35) Pieta, I. S.; Rathi, A.; Pieta, P.; Nowakowski, R.; Hołdyski, M.; Pisarek, M.; Kaminska, A.; Gawande, M. B.; Zboril, R. Electrocatalytic methanol oxidation over Cu, Ni and bimetallic Cu-Ni nanoparticles supported on graphitic carbon nitride. *Appl. Catal. B* **2019**, *244*, 272-283.
- (36) Zhang, P.; Dai, X.; Zhang, X.; Chen, Z.; Yang, Y.; Sun, H.; Wang, X.; Wang, H.; Wang, M.; Su, H.; Li, D.; Li, X.; Qin, Y. One-Pot Synthesis of Ternary Pt–Ni–Cu Nanocrystals with High Catalytic Performance. *Chem. Mater.* **2015**, *27*, 6402-6410.
- (37) Ying, J.; Jiang, G.; Cano, Z. P.; Ma, Z.; Chen, Z. Spontaneous weaving: 3D porous PtCu networks with ultrathin jagged nanowires for highly efficient oxygen reduction reaction. *Appl. Catal. B* **2018**, *236*, 359-367.

- (38) Qin, Y.; Zhang, X.; Dai, X.; Sun, H.; Yang, Y.; Li, X.; Shi, Q.; Gao, D.; Wang, H.; Yu, N.-F.; Sun, S.-G. Graphene Oxide-Assisted Synthesis of Pt–Co Alloy Nanocrystals with High-Index Facets and Enhanced Electrocatalytic Properties. *Small* **2016**, *12*, 524-533.
- (39) Wu, P.; Zhang, H.; Qian, Y.; Hu, Y.; Zhang, H.; Cai, C. Composition- and Aspect-Ratio-Dependent Electrocatalytic Performances of One-Dimensional Aligned Pt–Ni Nanostructures. *J. Phys. Chem. C* **2013**, *117*, 19091-19100.
- (40) Kitchin, J. R.; Nørskov, J. K.; Barteau, M. A.; Chen, J. G. Modification of the surface electronic and chemical properties of Pt(111) by subsurface 3d transition metals. *J. Chem. Phys.* **2004**, *120*, 10240-10246.
- (41) Gorzkowski, M. T.; Lewera, A. Probing the Limits of d-Band Center Theory: Electronic and Electrocatalytic Properties of Pd-Shell–Pt-Core Nanoparticles. *J. Phys. Chem. C* **2015**, *119*, 18389-18395.
- (42) Luo, M.; Zhao, Z.; Zhang, Y.; Sun, Y.; Xing, Y.; Lv, F.; Yang, Y.; Zhang, X.; Hwang, S.; Qin, Y.; Ma, J.-Y.; Lin, F.; Su, D.; Lu, G.; Guo, S., PdMo bimetallic for oxygen reduction catalysis. *Nature* **2019**, *574*, 81-85.
- (43) Matin, M.; Lee, E.; Kim, H.; Yoon, W.-S.; Kwon, Y.-U., Rational syntheses of core–shell Fe@(PtRu) nanoparticle electrocatalysts for the methanol oxidation reaction with complete suppression of CO-poisoning and highly enhanced activity. *J. Mater. Chem. A* **2015**, *3*, 17154-17164.
- (44) Jinchang, F.; Qi, K.; Zhang, L.; Zhang, H.; Yu, S.; Cui, X. Engineering the Pt/Pd Interfacial Electronic Structures for Highly-efficient Hydrogen Evolution and Alcohol Oxidation. *ACS Appl. Mater. Inter.* **2017**, *9*, 18008-18014.
- (45) Huang, W.; Wang, H.; Zhou, J.; Wang, J.; Duchesne, P. N.; Muir, D.; Zhang, P.; Han, N.;

Zhao, F.; Zeng, M.; Zhong, J.; Jin, C.; Li, Y.; Lee, S.-T.; Dai, H. Highly active and durable methanol oxidation electrocatalyst based on the synergy of platinum–nickel hydroxide–graphene. *Nat. Commun.* **2015**, *6*, 10035.

(46) Wang, Y.; Wu, B.; Gao, Y.; Tang, Y.; Lu, T.; Xing, W.; Liu, C. Kinetic study of formic acid oxidation on carbon supported Pd electrocatalyst. *J. Power Sources* **2009**, *192*, 372-375.

(47) Huang, L.; Han, Y.; Zhang, X.; Fang, Y.; Dong, S. One-step synthesis of ultrathin Pt x Pb nerve-like nanowires as robust catalysts for enhanced methanol electrooxidation. *Nanoscale* **2016**, *9*, 201-207

(48) Peng, Z.; Yang, H. PtAu bimetallic heteronanostructures made by post-synthesis modification of Pt-on-Au nanoparticles. *Nano Res.* **2009**, *2*, 406-415.

(49) Tang, M.; Luo, S.; Wang, K.; Du, H.; Sriphathoorat, R.; Shen, P. Simultaneous formation of trimetallic Pt-Ni-Cu excavated rhombic dodecahedrons with enhanced catalytic performance for the methanol oxidation reaction. *Nano Res.* **2018**, *11*, 4786-4795.

(50) Cao, Y.; Yang, Y.; Shan, Y.; Huang, Z. One-Pot and Facile Fabrication of Hierarchical Branched Pt–Cu Nanoparticles as Excellent Electrocatalysts for Direct Methanol Fuel Cells. *ACS Appl. Mater. Inter.* **2016**, *8*, 5998-6003.

(51) Obradović, M. D.; Rogan, J.; Babic, B.; Tripković, A. V.; Gautam, A. R. S.; Radmilović, V. R.; Gojkovic, S. Formic acid oxidation on Pt-Au nanoparticles: Relation between the catalyst activity and the poisoning rate. *J. Power Sources* **2012**, *197*, 72-79.

## Graphical Table of Content (TOC)

